Journal of Applied Fluid Mechanics, Vol. 18, No. 9, pp. 2212-2225, 2025.
Available online at www.jafmonline.net, ISSN 1735-3572, EISSN 1735-3645.
https://doi.org/10.47176/jafm.18.9.3387

Numerical Investigation of the Impact of a Hollow Ceramic Droplet on Metallic Substrate

M. Driouche[1†], T. Rezoug[1] and M. El Ganaoui[2]

[1] *Blida 1 University, Institute of Aeronautics and Space Studies, Laboratory of Aeronautical Sciences, BP 270, Souma Road 09100, Algeria*
[2] *LERMAB, IUT of Longwy, Lorraine University, France*

†*Corresponding Author Email: driouche_mouloud@univ-blida.dz*

ABSTRACT

The objective of this study is to numerically investigate the spreading and solidification of a hollow ceramic droplet impacting a metallic substrate, with a particular focus on the melting of the substrate. The numerical model employs the PISO (Pressure-Implicit with Splitting of Operators) algorithm to solve the equations governing transient fluid dynamics, utilizing the pressure-based finite volume method in a 2D axisymmetric domain. The volume of fluid (VOF) method is employed to ensure the tracking of the droplet/air interface during spreading and solidification. The enthalpy porosity method is utilized for the monitoring of the liquid/solid interface throughout the processes of droplet solidification and substrate melting. The interaction between the spreading droplet and the substrate is represented by a thermal contact resistance. To validate the hollow droplet impact model, a comparison with published experimental results was performed. Simulations were conducted under plasma spray conditions for varying initial droplet temperatures and contact thermal resistances to assess their influences on droplet spreading and solidification, as well as substrate melting. It was observed that the initial droplet temperature significantly affects the splat morphology and substrate melting. However, thermal contact resistance exerts a greater influence on substrate melting than on the final splat shape. Thus, it was found that the droplets, whose initial temperature is high, impacting the substrates with low thermal contact resistance, improve the adhesion of the coatings.

Article History

Received January 19, 2025
Revised April 10 2025
Accepted May 1, 2025
Available online July 5, 2025

Keywords:

Hollow droplet
Spreading
Solidification
Substrate melting
Computational fluid dynamics

1. INTRODUCTION

Many industrial applications use the impact of droplets on a solid surface, such as thermal spray coating, hot surface cooling, in-flight icing, inkjet printing, spray painting and chemical process (Labergue et al., 2015; Latka et al., 2020; Zhong et al., 2020; Xu et al., 2022; Niu et al., 2023; Chen et al., 2024, 2025). Plasma spray coatings protect components from corrosion, oxidation, wear and extreme temperatures. The quality of the coating is largely determined by the fluid flow, heat transfer and solidification as the droplets spread over the substrate (Tejero-Martin et al., 2019). Many studies have been devoted to understanding the formation of coatings, most of which have been carried out using numerical models (Emdadi & Pournaderi, 2019; 2020; Shen et al., 2020; Bobzin et al., 2023) due to the difficulty of observing on the scale of micrometers and micron seconds (Goutier et al., 2012). For several reasons, dense droplets may not be completely melted during their stay in the thermal jet, which significantly affects the quality of the coating (Alavi et al., 2012). Hollow droplets have therefore recently been studied because the vacuum initially present in the particles influences their behaviour in flight before impacting, such as speed and melting. The particles melt completely, resulting in a uniform temperature throughout the hollow droplet (Kamnis et al., 2011). Hollow droplet coatings open new possibilities with improved properties such as adhesion, structure and controlled porosity (Solonenko et al., 2008a, b). By controlling the porosity of coatings, it is possible to produce coatings with improved thermal insulation properties, such as thermal barrier coatings (TBCs) used in turbine blades. Hollow particles of metals, alloys, oxides and other ceramics can be produced by plasma treatment of various powder materials (Safaei & Emami, 2017).

Compared with studies on dense droplets, there are only a few studies in the literature devoted to hollow droplets (Blanken et al., 2021). Gulyaev et al. (2009) were the first to observe the formation of a central counter jet resulting from the spreading of a hollow droplet. In a separate study, they present experimental results on the spreading and formation of a counter jet when a hollow glycerine droplet is impacted under typical plasma projection conditions. They also developed a simple theoretical model to assess the fluid dynamics (Gulyaev & Solonenko, 2013). Kumar et al. (2012) numerically simulated the impact of a millimeter-sized glycerine droplet on a solid surface. They showed that a high impact velocity leads to a significant height of the central counter jet. In another study (Kumar et al., 2013), they extended their model by introducing heat transfer and solidification to study the impact of a hollow ZrO2 droplet. They reported that the final spreading diameter is smaller compared to that of a dense droplet, unlike the solidification time, which is more important for a hollow droplet. Safaei et al. (2017) numerically simulated the impact of a ZrO2 droplet, considering compressible flow. Their results were compared with experimental results. They showed that at high impact velocities, the compression of the gas trapped inside the droplet significantly affects the impact dynamics and the structure of the droplet. Xiaogang et al. (2023) used the level-set method combined with the Volume of Fluid (VOF) approach in a 2D axisymmetric domain to study and compare the effects of dense and hollow molten ZrO2 droplets on both a dry substrate and an already solidified layer. They found that the final spreading diameter of a dense droplet is larger than that of a hollow droplet due to the formation of a counter jet. An et al. (2024) numerically studied the influence of impact velocity and substrate temperature on the spreading of a hollow metal droplet colliding with a cold substrate. They found that solidification modifies the spread of the droplet as well as the formation of the central counter jet. Their simulations showed that solidification could slow down the formation of the counter jet. The maximum diameters predicted by the simulations are in good agreement with a quantitative analysis, which they established by setting up an energy conservation equation.

A notable rise in substrate temperature has the potential to result in the melting of the surface. This permits a further improvement in the metallurgical bond between the initial coating layers and the substrate, thus enhancing the overall quality of the coating. Experimental and numerical studies have been conducted with the objective of enhancing comprehension of this phenomenon. Shigeru and Atsushi (1974) observed the formation of intermetallic compounds at initials layers in specific droplet-substrate combinations. The formation of intermetallic compounds is a consequence of substrate melting, which has the potential to significantly influences the coating's adhesion. In their experimental study, Li et al. (2006) investigated the effect of substrate melting on the splat structure. they observed that the splashing of droplets was a consequence of local melting of the substrate. This type of splashing could not be circumvented by preheating the substrate. Li et al. (2004) investigated the effect of substrate melting and resolidification during thermal spraying experimentally and numerically for various droplet and substrate combinations. They demonstrated by experimental evidence that the characteristics of the droplet and substrate played a significant role in substrate melting. Driouche et al. (2019) developed a computational fluid dynamics (CFD) model to study the substrate melting phenomenon that occurs when a molten ceramic droplet strikes a metal substrate. In addition, the effect of droplet size on substrate melting was examined. The authors concluded that for a large droplet size, substrate melting is important, which positively affects coating quality. In the above studies, only dense droplets were considered. A review of the literature reveals that only Patel et al. (2022) investigated substrate melting in the context of hollow droplet impact. The analysis was carried out using in-house code written in FORTRAN 95. The results indicate that an increase in the initial temperature and impact velocity of the hollow droplet leads to a greater melting depth and diameter. This suggests that hollow droplets are preferable to dense droplets for good coating quality.

A review of the literature on the impact of hollow droplets in the thermal spraying process reveals a dearth of rigorous examination of this issue, particularly regarding the phenomenon of substrate melting, which influences the quality of the coatings. This paper examines the effect of the initial temperature of a hollow alumina (Al2O3) droplet impacting a stainless-steel substrate, as well as the influence of thermal contact resistance on the splat morphology and substrate melting, under conditions of plasma projection. The fluid dynamics equations and the energy equation, which includes the liquid/solid phase change, were solved using the CFD method using ANSYS FLUENT 16 software (Ansys Inc, 2016).

2. NUMERICAL MODELLING

In this study the impact of a hollow alumina droplet on a stainless-steel substrate, with a focus on the effects of substrate melting, was analysed. As shown in Fig. 1, a completely spherical hollow droplet of alumina impacts onto the substrate initially at 650 K, with a vertical velocity of 75 m/s. The external diameter of the droplet (D_0) is 50.8 µm, and the internal diameter of the air cavity (D_i) is 40.6 µm. This results in an equivalent diameter ($D_{eq} = \sqrt[3]{D_0^3 - D_i^3}$) of a dense droplet with the same mass, which is 40 µm. These diameters are chosen for a relative thickness ($\delta = (D_0 - D_i)/2D_0$) equal to 0.1, which reflects the plasma projection conditions (Gulyaev et al., 2009). The initial droplet temperature and the thermal contact resistance were varied, to examine their influences on droplet spreading and substrate melting. Under these conditions the Reynolds number ($Re = \rho_g V_0 D_0/\mu_g$, where ρ_g: droplet density; V_0: impact velocity; D_0: initial diameter and μ_g: dynamic viscosity) and Weber number ($We = \rho_g V_0^2 D_0/\sigma$, where σ: surface tension) have values of 370 and 1652 respectively. This confirms that the flow is laminar and that capillary effects are negligible (We≫√Re) (Pasandideh-Fard et al., 1996). The transient

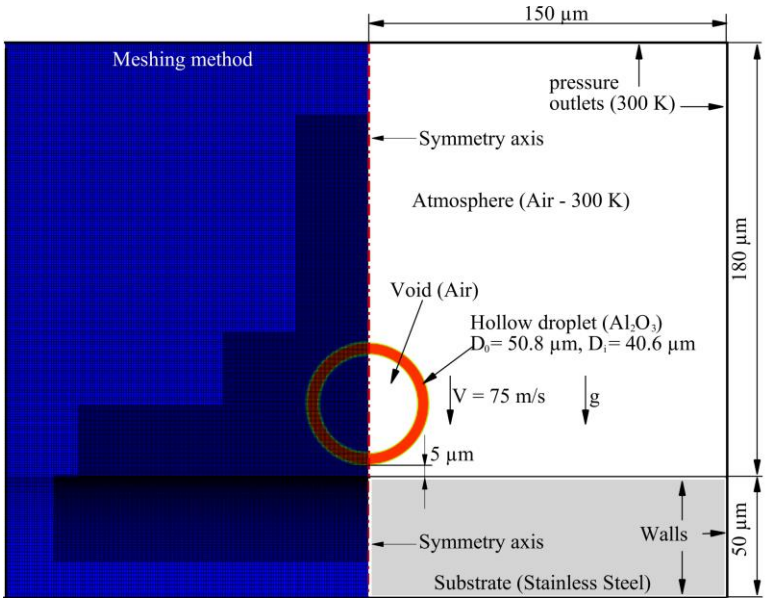

Fig. 1 2D Axisymmetric domain for the simulation and meshing method

Table 1 Thermo-physical properties of the droplet and substrate (Kumar et al., 2013; Keshri & Agarwal, 2011)

Properties	Alumina (Al2O3)	Stainless Steel
Density (kg/m^3)	3990	7900
Thermal conductivity (W/m K) (sol)	5.9	14.9
Thermal conductivity (W/m K) (liq)	7.86	14.9
Specific heat (J/kg K) (sol)	1273	477
Specific heat (J/kg K) (liq)	1358	477
Kinematic viscosity (m^2/s)	1.03x10^{-5}	
Surface tension (N/m)	0.69	
Melting Point (K)	2327	1723
Latent heat of fusion (J/kg)	1.16x10^6	2.6x10^5

fluid dynamics and energy equations, accounting for the liquid/solid phase change, were solved in a 2D axisymmetric domain using the finite volume method. The air/liquid interface was captured by the volume of fluid (VOF) method. The surface tension at the boundary between the droplet and the air was modelled by the (CSF) "Continuum Surface Force" method, initiated by Brackbill et al. (1992). To simulate the solidification of the droplet and the melting of the substrate, the porosity-enthalpy method (Voller & Prakash, 1987) was employed. The deformation of the substrate during its melting is not considered in this study. More details describing the equations used in this model, can be found in our previous work (Driouche et al., 2019).

As illustrated in Fig. 1, the outer boundaries of the droplet domain are treated as pressure outlets and kept at a temperature of 300 K. Similarly, the substrate walls are maintained at 300 K, the contact angle between the droplet and the substrate is kept constant at 90°. The thermo-physical properties of alumina and stainless steel are detailed in Table 1.

In this model, a structured grid was adopted using the CPR parameter (Cell Per Radius). Two mesh areas have been defined in order to reduce the calculation time.

The first area is relatively coarse, while the second area is very fine where high gradients are expected. This

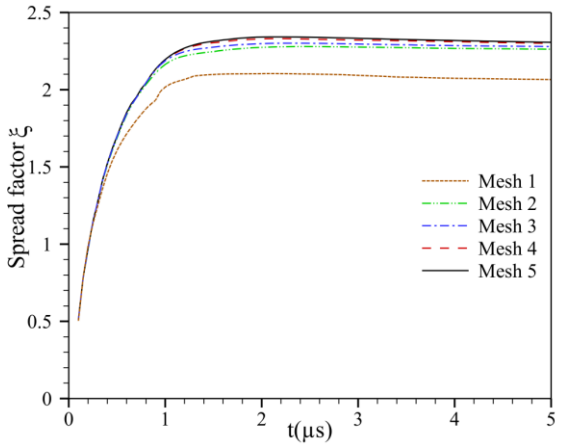

Fig. 2 Temporal variation of the spreading factor of the hollow alumina droplet with five different meshes

corresponds to the droplet impact zone and the droplet/substrate interface, as shown in Fig. 1. In order to verify the independence of the grid, five different meshes were tested. For each mesh, a value of CPR is retained for the coarse zone and 2xCPR for the fine zone, namely:

Mesh 1 (10-20), Mesh 2 (15-30), Mesh 3 (20-40), Mesh 4 (25-50), Mesh 5 (30-60). Figure 2 illustrates the

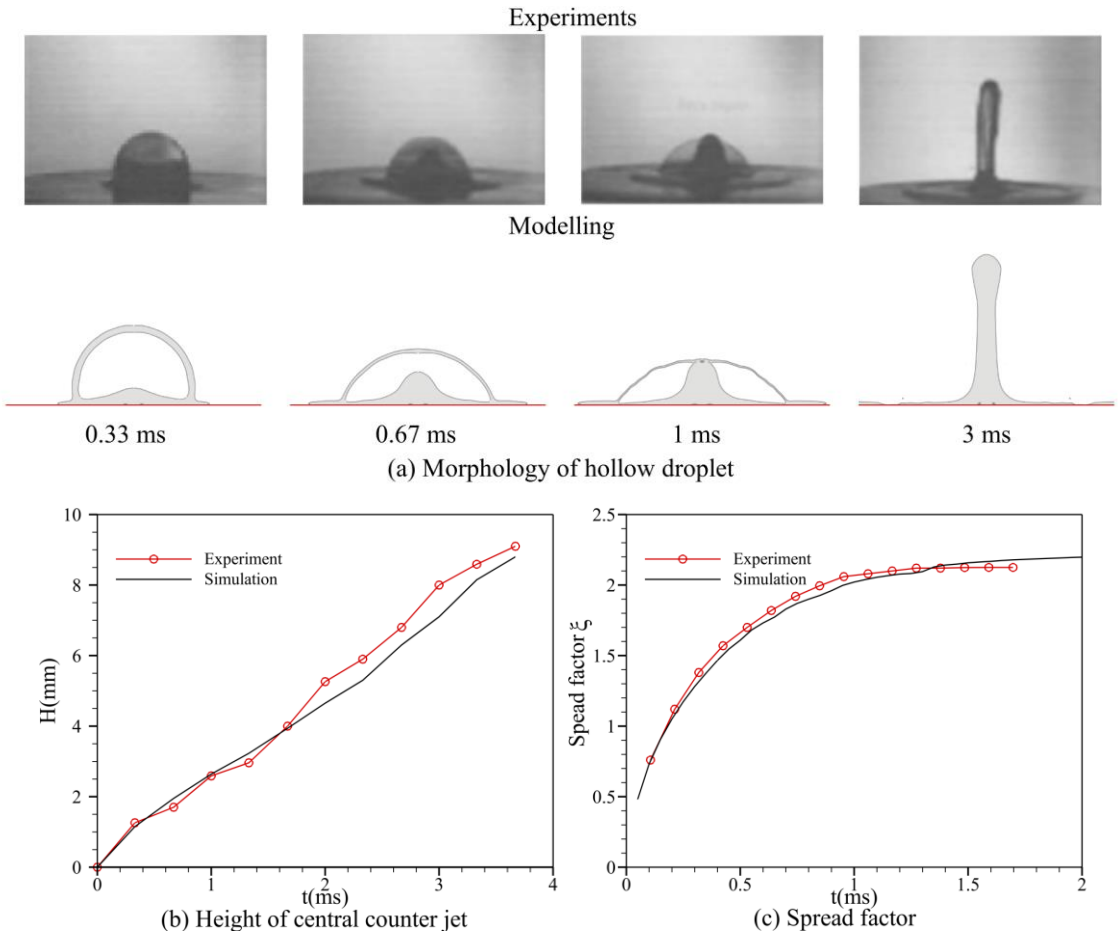

Fig. 3 Comparison of simulation and experiment (Gulyaev & Solonenko, 2013) results for impact of a hollow glycerin droplet

evolution of the spreading factor of the hollow alumina droplet at an initial temperature of 3000 K, considering a contact thermal resistance of 10-8 m2KW-1 for different grids. It is observed that the curves gradually overlap as the CPR increases. Considering the computation time and numerical accuracy, Mesh 4 (25-50) was selected for this model.

The PISO algorithm was employed to couple pressure and velocity, and the QUICK scheme was applied to solve the energy and momentum equations. The Geo-Reconstruct scheme, which relies on geometric data, was used to track the interface between the droplet and air. The PRESTO! scheme was used for pressure interpolation. A constant time step ranging from 10^{-11} to 10^{-9} seconds was selected for the first-order implicit formulation.

The proposed model has previously been validated for the impact of dense droplets in prior studies (Driouche et al., 2019, 2020). In this study, the simulation results obtained by this model were compared with experimental results in the case of impact of a hollow droplet on a solid surface, carried out by Gulyaev and Solonenko (2013). The experimental conditions were meticulously designed to consider fluid dynamics exclusively, while disregarding heat transfer and phase change. The impact of a hollow spherical droplet of molten glycerin, with an outer diameter of 5.25 mm and an inner vacuum (air) diameter of 4.389 mm, on a solid surface at a velocity of 5.94 m/s was considered. As illustrated in Fig. 2, strong agreement between the experimental results and the predictions made by the presented model. The simulation accurately predicted the occurrence of the central counter jet phenomenon, as well as the rupture of the droplet shell at 1 ms. A quantitative comparison is also presented in Fig. 3, comparing the central counter jet height and the spread factor (ξ=diameter of spread/initial diameter). the simulated results are consistent with the experimental results. The spread factor reaches its maximum 2.1 at 1.5 ms is observed experimentally against 2.2 at 2 ms predicted by the model.

3. RESULTS AND DISCUSSIONS

Before studying the influence of initial droplet temperature and contact thermal resistance on droplet morphology and substrate melting, a detailed explanation of the mechanisms of droplet internal flow, heat transfer, droplet solidification and substrate melting was provided. This explanation has enabled to understand the phenomena that accompany the formation of coatings. For this reason, the impact of a droplet at 3,000 K and a contact thermal resistance of 10^{-8} m^2KW^{-1} were used for this explanation.

Figure 4 shows the pressure field (left) and velocity field, as well as the streamlines (right), at different times.

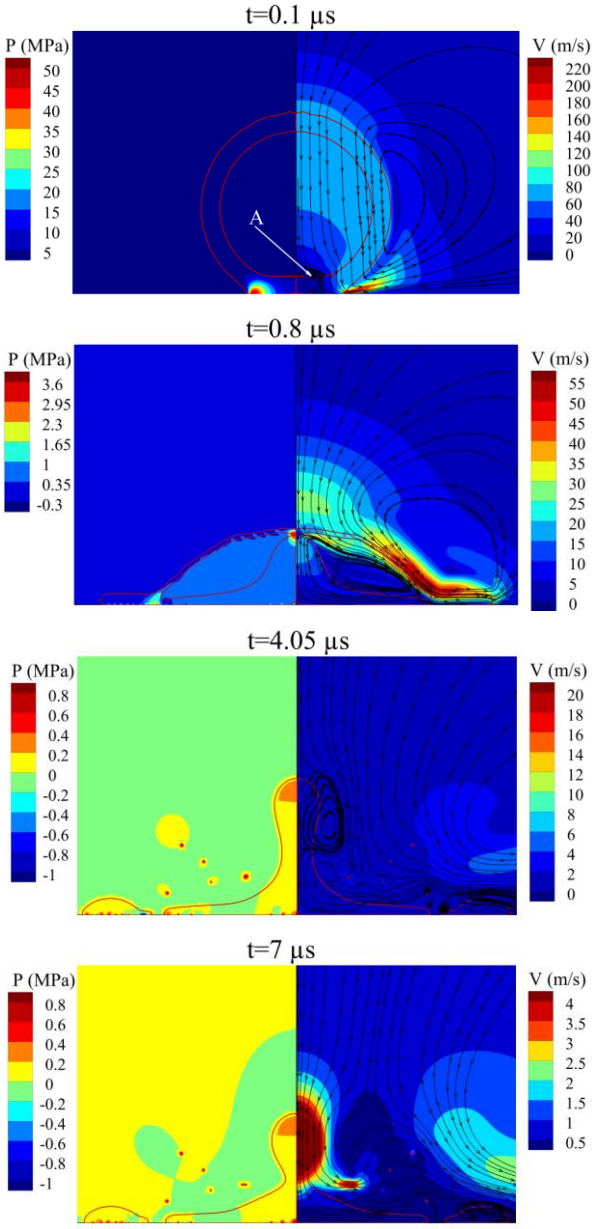

Fig. 4 Pressure field (left) and velocity field as well as streamlines during the impact of a hollow alumina droplet at 3000 K at different times

It should be noted that, following impact (t=0.1 µs), the kinetic energy metamorphoses into potential energy, leading to a significant increase in pressure near the centre of the droplet (50 MPa). This increase in pressure creates a pressure gradient between the centre of the droplet and its edge. This gradient causes the droplet to spread in a radial direction, resulting in a significant increase in flow velocity, which can reach three times the initial velocity, i.e. 220 m/s. This gradient induces the formation of an outward vortex, driving out the adjacent air. The formation of an additional vortex, designated here by the letter A, takes place close to the centre of the droplet due to the pressure gradient and the internal vacuum. This dynamic contributes to the supply of liquid to the centre of the droplet from the upper part, leading to the formation of the central counter jet. At 0.8 µs, the feeding of the spread part of the droplet and the counter jet leads to a reduction in the size of the upper shell. At the same time, the internal vortex intensifies, while the counter jet progresses until it reaches the upper part of the shell. Later (4.05 µs), the central counter jet reaches its maximum height, with the appearance of a throttling in the middle, which is due to the first vortex still inducing the upflow and another downflow caused by another vortex in the opposite direction. At 7 µs, the counter-jet begins its descent onto the lower part of the droplet, which has completed its spreading. Once the kinetic energy is completely dissipated, the surface tension exerts a force on the edges of the droplet, pushing them back towards the centre. This dynamic causes a small-amplitude vortex to form.

It is essential to note that, immediately after impact, the significant difference in temperature between the droplet (3000 K) and the substrate (650 K) induces significant and rapid heat transfer from the droplet to the substrate. In the proposed model, conduction and convection are the only transfer modes taken into account. As shown in Fig. 5, considerable heat flow is observed at the surface of the contact, between the droplet and the substrate (6 x 10^{10} W/m^2) at 0.1 µs. The temperature rises to 1850 K, due to the entrapment of air between the droplet and the substrate, heat transfer is disrupted in these regions, resulting in fluctuations in temperature and heat flux. The flow velocity is slowed at the substrate surface due to the solidification process, leading to an increase in conductive heat transfer. At times of 0.3 µs and 1 µs, spreading and solidification progress. Solidification leads to a reduction in the heat flux, although it is higher at the droplet edge due to the presence of fewer solid layers. On the other hand, fluctuations are more marked, again due to the trapping of air induced by solidification, which disturbs the flow. Complete solidification of the lower part of the droplet is observed at 4.05 µs. The heat flux decreases practically along the surface, but the temperature is maintained at around 1800 K, except at the point where the droplet broke off (1300 K).

The solidification of the droplet and the melting of the substrate are modelled using an enthalpy formulation. This approach makes it possible to determine the liquid fraction in each cell and to define an intermediate mushy zone between the liquid and solid phases.

Upon droplet impact and after heat transfer from the droplet to the substrate, the droplet cools until it reaches the melting point (2327 K), marking the start of solidification. According to Fig. 6, at time 0.2 µs, the liquid fraction of the droplet (alumina) located in the lower part is between 0 and 1, marking the start of solidification and the formation of the mushy zone. At this stage, the substrate is heated, but not to the melting point (1723 K), which corresponds to the solid state, characterized by a zero liquid fraction. At 0.4 µs, much of the lower part of the droplet is solidified, with the exception of the edge.

The region of the substrate between 13 µm and 24 µm initiates a melting process, as the liquid fraction at this point approaches unity. At the same time, progressive spreading and cooling of the droplet induces progressive solidification throughout the lower part, with the exception of the counter jet region, which, being far from the substrate surface, is, consequently less exposed

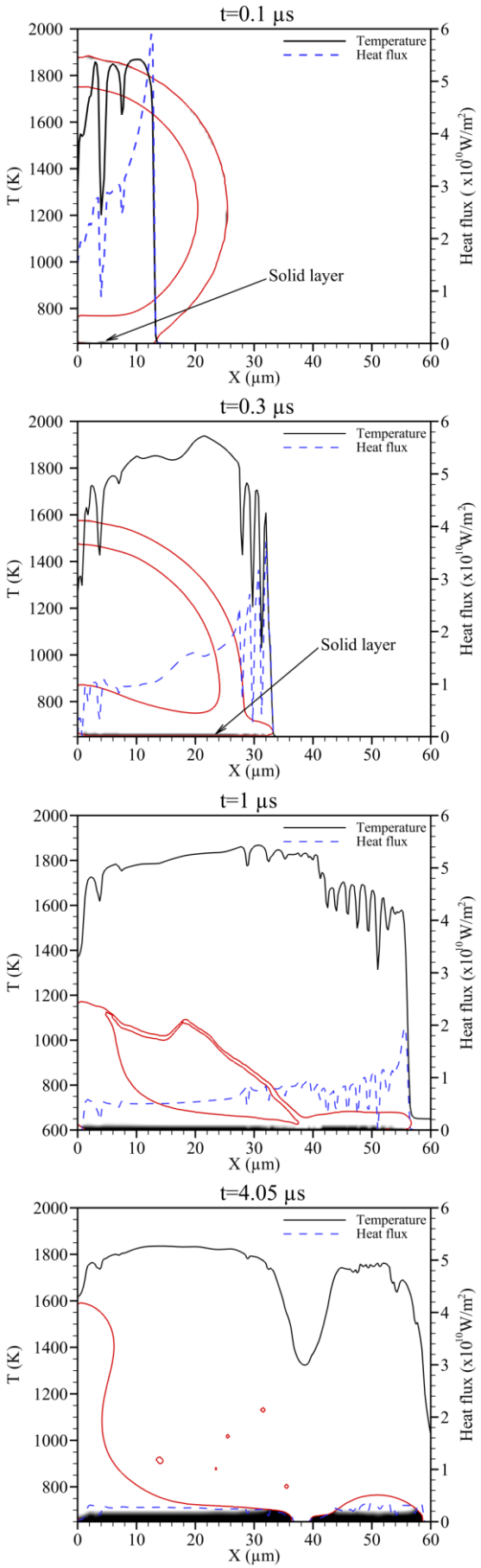

Fig. 5 Heat flux and temperature distribution along the substrate surface during the impact of a hollow alumina droplet at 3000 K at different times

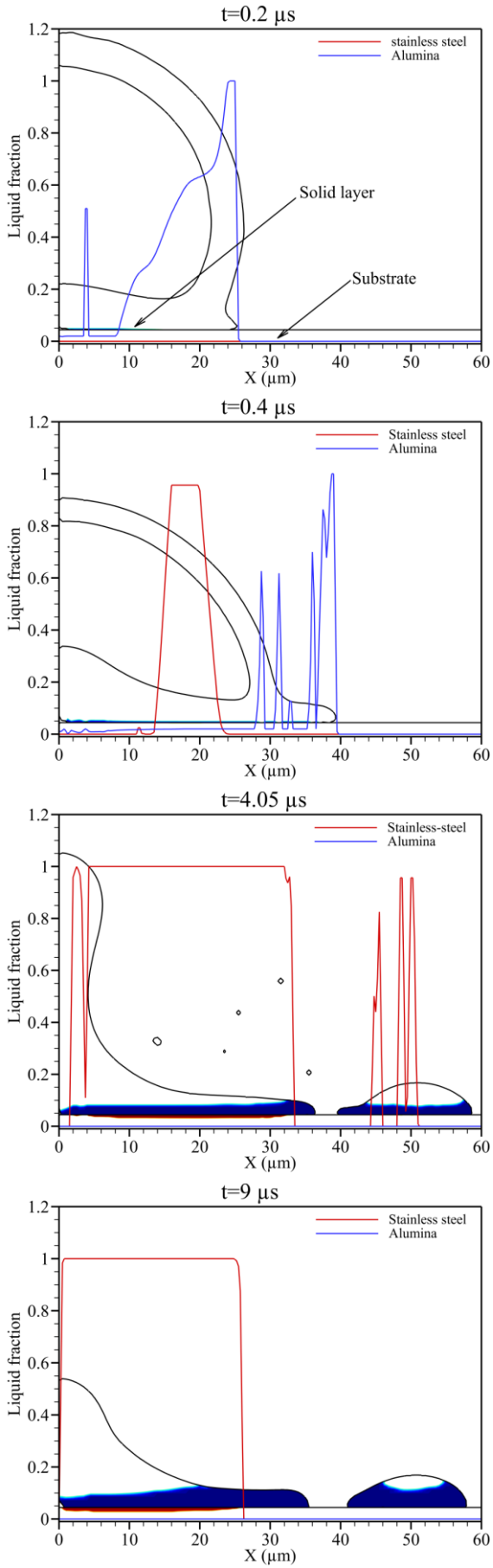

Fig. 6 Solidification of the droplet and melting of the substrate during the impact of a hollow alumina droplet at 3000 K at different times

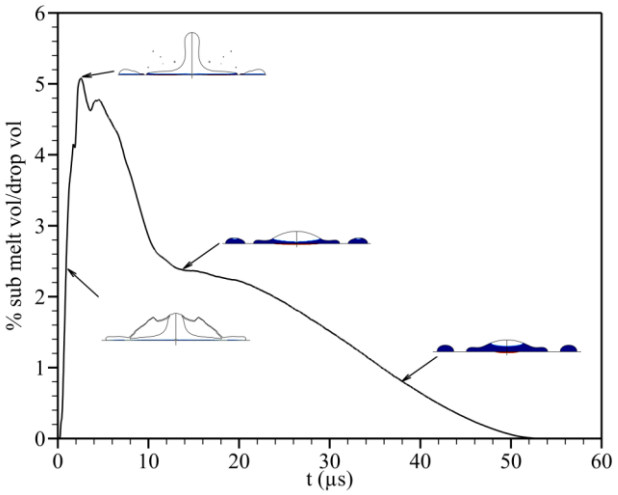

Fig. 7 Temporal evolution of the melted substrate volume, case of alumina droplet impact (3000 K)

to cooling. On the other hand, the substrate is subjected to intense heat, inducing melting that spreads radially and in depth. After a period of time (9 µs), the top of the substrate begins to cool by releasing heat to depth, but slowly due to its low conductivity, and the substrate begins to solidify again.

As shown in Fig. 7, the volume of molten substrate peaks at 2.56 µs and then declines rapidly. From 13.5 µs onwards, substrate melting is maintained at an almost constant level by the counter jet, which falls back and begins to cool by transferring heat to the substrate. Final solidification of the substrate does not occur until 53.1 µs, marking a significant period when adhesion between the splat and the substrate may be compromised.

3.1 Influence of the Initial Droplet Temperature

The initial temperature was varied from 2600 (K) to 3200 K, in steps of 200 K. A thermal contact resistance of 10^{-8} m^2KW^{-1} was maintained throughout the simulation. As illustrated in Fig. 8, the impact, spreading, and temperature distribution of the droplets are observed. Each image in the figure corresponds to a specific temperature, with the left side depicting the droplet impact at 2600 K and the right side showing the impact at 3000 K. At the initial time of 0 µs, both droplets are positioned 5 µm above the surface. Upon impact, the lower part of the droplet begins to spread radially due to kinetic energy, while the upper part exhibits deformation in both the shell

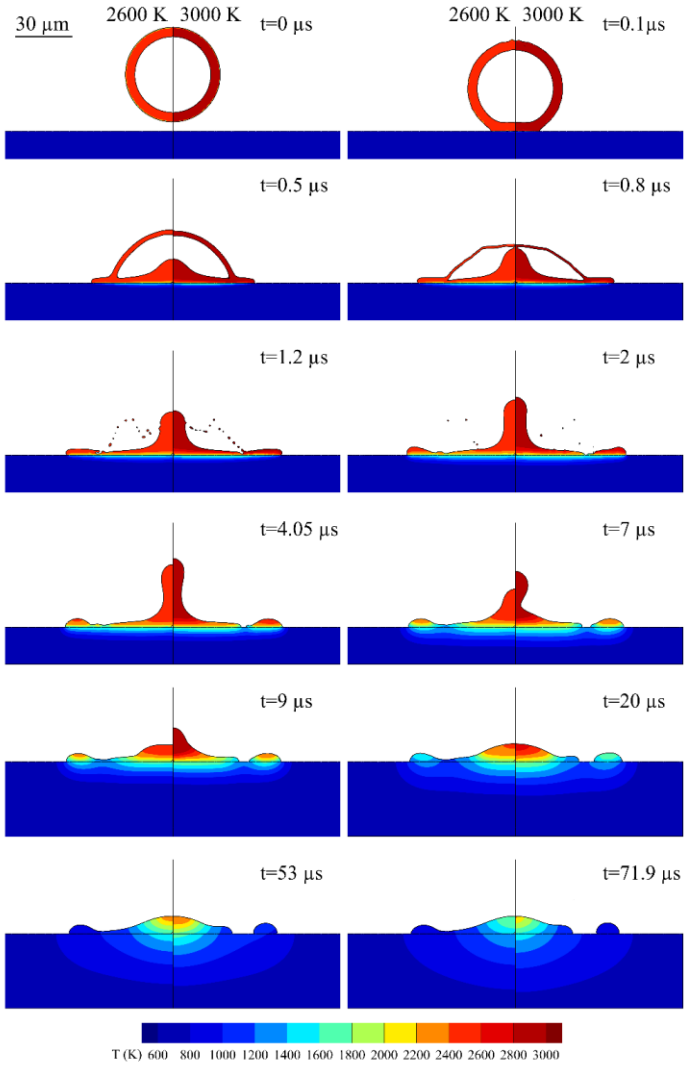

Fig. 8 Droplet spreading and temperature distribution, for an initial droplet temperature of 2600 K (left) and 3000 K (right)

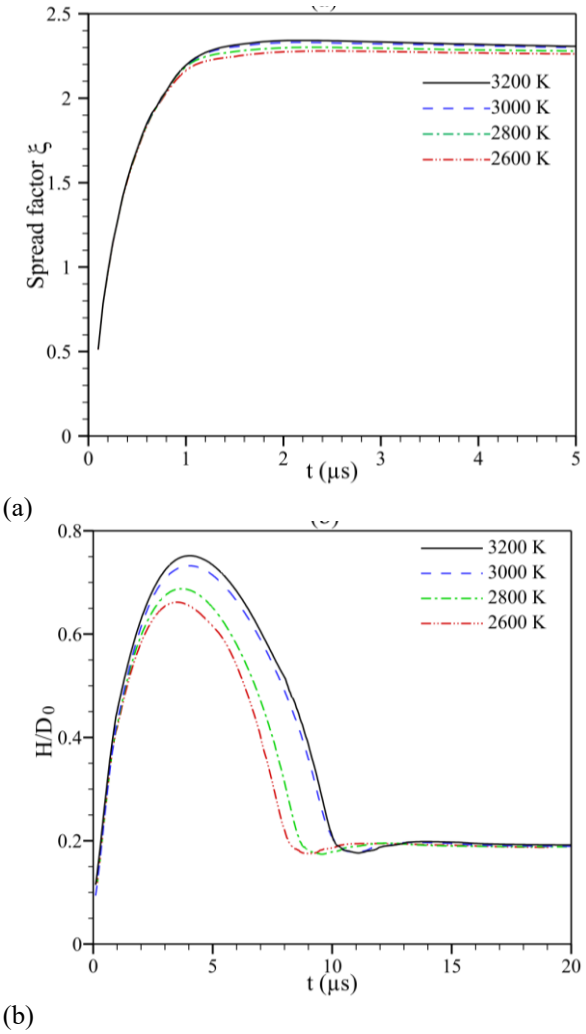

Fig. 9 Temporal variation of the spread factor (a) and the relative height of the central counter jet (b), for different initial droplet temperatures

and the empty cavity. This deformation involves outward stretching of the empty cavity and thinning of the shell, observable in both droplets at 0.5 µs, concurrently, the appearance of a central counter jet was observed. This phenomenon aligns with the observations reported in the experimental study by Gulyaev and Solonenko (2013).

The shell undergoes a continued stretching process, and the central counter jet displaces until they meet at 0.8 µs. Subsequently, the shell ruptures at 1.2 µs. It is noteworthy that the central counter jet of the droplet initially at 3000 K exhibits a greater upward movement compared to the droplet initially at 2600 K. These results in a maximum height reached at 4.05 µs, after which the central counter jet initiates a descent along the lower portion of the droplet. For the droplet initially at 3000 K, the central counter jet requires a longer time to fall back, as evidenced at 7 µs and 9 µs, in contrast to the droplet initially at 2600 K. Another phenomenon observed with the drop initially at 3000 K is the detachment of the end of the portion spread out on the substrate at 2 µs. The causes of this detachment will be discussed in Fig. 11. The droplet initially at 2600 K, after its total spreading, adopts a singular splat configuration, characterized by increased thickness at its center and rounded edges. This shape is due to surface tension, which causes the flow to retreat towards the center after kinetic energy is exhausted. In contrast, the splat of the second drop is composed of two distinct parts. The central part of the splat is comparatively thick, while the second part, located slightly further out, makes up 22.3% of the entire splat. This can help optimize the plasma spray coating for the desired properties.

According to Fig. 8, a heat transfer occurs immediately after the two droplets hit the substrate, causing the cooling of the lower part of the droplets in contact with the substrate. The droplet initially at 2600 K cools more rapidly. Conversely, the central zone of the counter jet remains at almost its initial temperature, since it is far from the substrate. This part of the droplet only begins to cool after falling back beyond 9 µs. Due to the low thermal conductivity of the stainless-steel substrate, droplets cool relatively slowly. The droplet initially at 3000 K transfers more heat both in depth and in the radial direction of the substrate.

Figure 9a shows the temporal variation of the spread factor for various initial droplet temperatures. The spread factor is defined as the ratio between the diameter of the droplet's surface in contact with the substrate and its initial outer diameter ($\xi = D/D_0$). Spreading occurs rapidly to reach its maximum. The spreading factor is higher at higher initial temperatures, with values of 2.34 and 2.28 for initial temperatures of 3200 K and 2600 K respectively. This can be explained by the solidification process, which slows down spreading at low initial temperatures. Figure 9b illustrates the evolution of the relative height of the central counter jet (H/D_0) over time for different initial temperatures. this height is proportional to the initial temperature. it reaches values of 0.75 and 0.65 corresponding to initial temperatures of 3000 K and 2600 K, respectively. the same trend is observed for the fall time of the central counter jet. The final height, which will be the maximum thickness of the splat, is practically the same for all initial temperatures.

Figure 10a shows the temperature evolution on the bottom surface of the splat at 10 µm from the center. A drop in temperature is observed immediately after impact, approaching the melting point of alumina (2327 K), initiating solidification, followed by rapid cooling in all cases of the initial temperature. At time between 1 µs and 4 µs, the central counter jet moves upwards, so the mass of the droplet in contact with the substrate is low, which explains the rapid cooling. Beyond this point (5 µs - 15 µs), the temperature stabilizes relatively, and a slight increase is even observed for the initial temperature 3000 K and 3200 K, this is the effect of the central counter jet, which falls back with its initial temperature (Fig. 9b). Because of the contact thermal resistance and low thermal conductivity of the substrate, slow cooling is observed, but relatively rapid for the low initial droplet temperatures.

In Fig. 10b, the temperature profile at a point 10 µm from the center on the upper surface of the substrate is depicted. The temperature rises sharply after the droplet contacts the substrate. Starting from an initial temperature of 2600 K, the temperature increases but does not reach

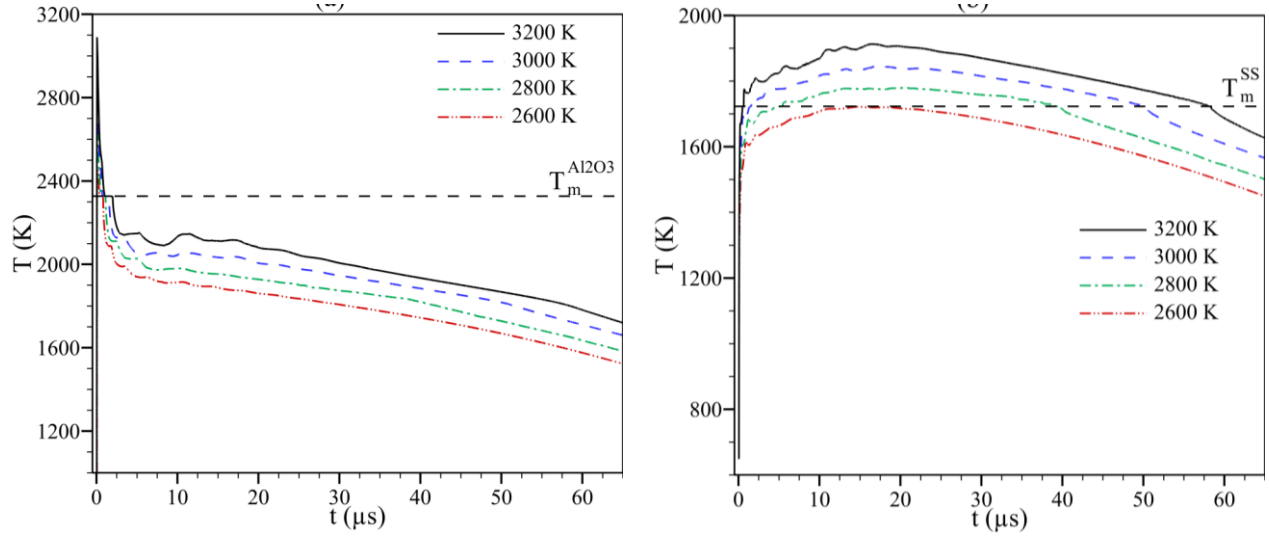

(a) (b)

Fig. 10 Temperature history of the lower surface of the droplet (a) and the upper surface of the substrate (b), for different initial droplet temperatures

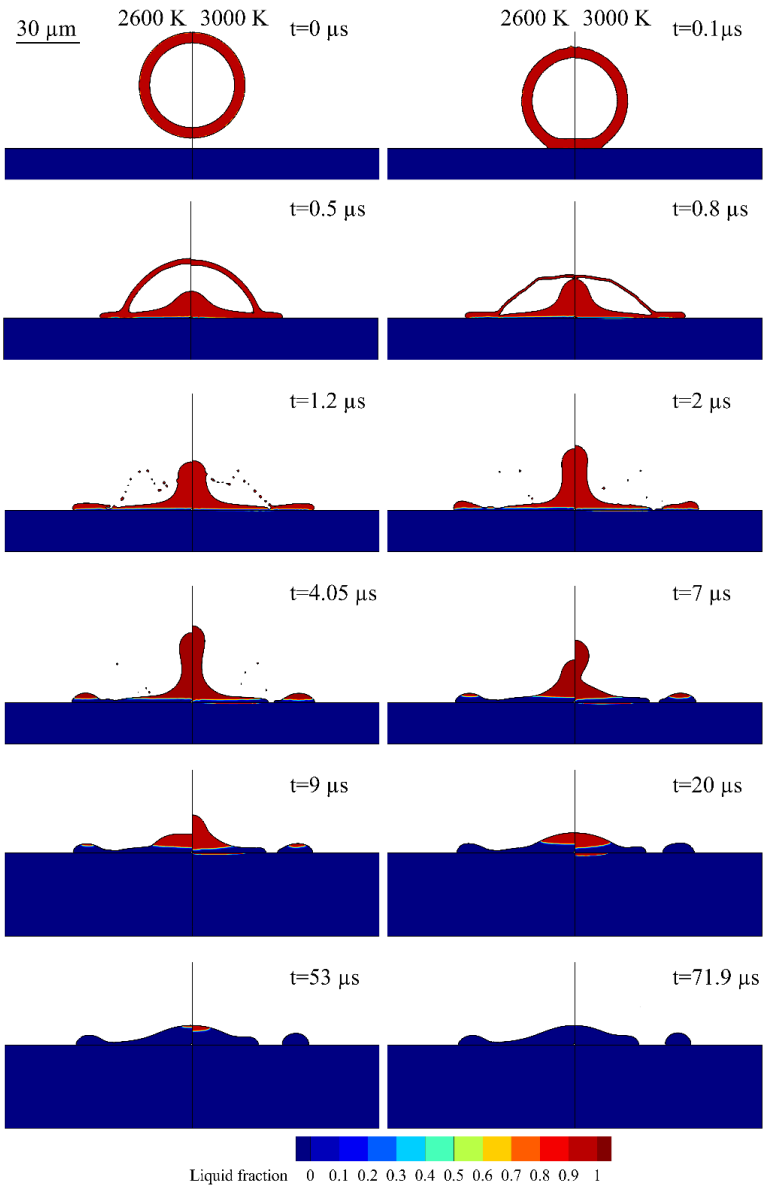

Fig. 11 Droplet solidification and substrate melting for an initial droplet temperature of 2600 K (left) and 3000 K (right)

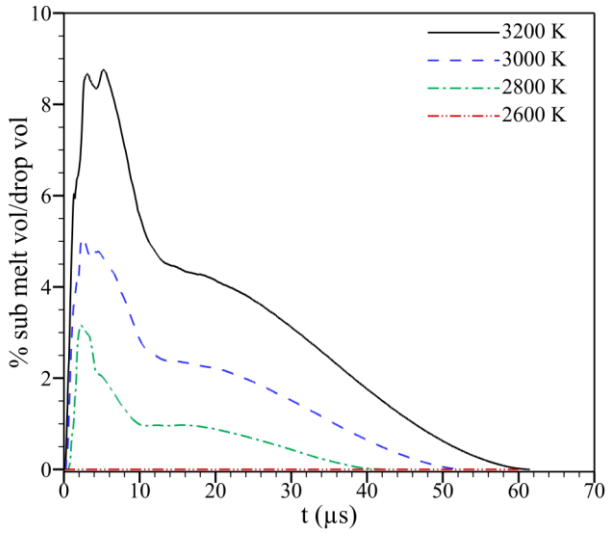

Fig. 12 Temporal evolution of the melted substrate volume, for different initial droplet temperatures

the melting point of 1723 K. Unlike the other temperatures (2800 K, 3000 K and 3200 K), the temperature exceeds the melting point, which induces substrate melting. The higher the initial droplet temperature, the more the substrate is heated. Moreover, the duration, which the temperature remains above the substrate's melting point, is directly proportional to this initial temperature, as it corresponds to 34.6 µs, 48.5 µs, and 57.6 µs for 2800 K, 3000 K, and 3200 K, respectively.

Figure 11 illustrates the solidification of the droplet and the melting of the substrate. The droplet solidifies immediately after impact. At 0.5 µs, the progress of solidification is faster for 2600 K than 3000 K is observed. At 2 µs for 2600K the central counter jet evolves more slowly because of the lower layer of the droplet which quickly solidifies and slows down the upward flow. Unlike for 3000 K, the non-solidified mass is greater, which favors upward flow. Additionally, the solidified layer is thinner at the droplet's end, enabling its detachment due to kinetic energy in the case of 3000 K. At 7 µs, solidification progresses from the droplet's end towards its center in both cases, as the central counter jet descends at this point, delaying solidification. The droplet for 2600 K solidifies completely at 53 µs vs 71.9 µs for 3000 K, the same observation that was made by Patel et al. (2022) for the significant solidification time caused by the central counter jet, is confirmed in this study. As discussed in Fig. 10b, no melting of the substrate is produced for 2600 K. The substrate starts to melt during the spreading process in the case of 3000 K, between 4 µs and 9 µs, the melting area is observed slightly away from the droplet's center, but it gradually shifts toward the center with a shallow depth. After 20 µs, melting progresses mainly in the center of the substrate with a relatively large depth, which is attributed to the movement of the central counter jet. The substrate then resolidifies after 53 µs.

The temporal evolution of the melt volume of the substrate relative to the volume of an equivalent dense droplet of 40 µm diameter and the same mass, for different

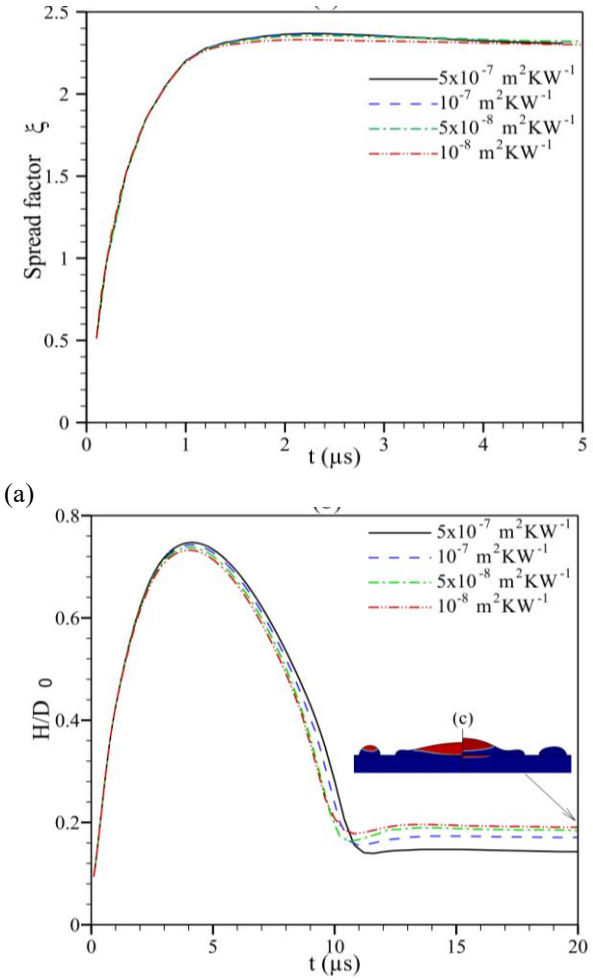

Fig. 13 Temporal variation of the spread factor (a) and the relative height of the central counter jet (b), for different thermal contact resistances

initial droplet temperatures is shown in Fig. 12. The melt volume of the substrate jumps rapidly to the maximum for each initial temperature, except 2600 K where melting does not occur. Then the melted volume decreases rapidly until the central counter jet falls, then the volume continues to decrease but for a long time, until the overall resolidification of the substrate. The melt volume and the melting period are proportional to the initial droplet temperature. The maximum volume equal to 3.16%, 5.1% and 8.76% respectively for 2800 K, 3000 K and 3200 K, the overall time for the substrate melting is 42.4 µs, 53.1 µs and 61.5 µs respectively. For a high temperature, the melting and its period are considerable, which promotes good adhesion between the spread hollow droplet and the substrate.

3.2 Influence of Thermal Contact Resistance

The thermal contact resistance was varied from $10^{-8}\,m^2KW^{-1}$ up to $5x10^{-7}\,m^2KW^{-1}$. The initial droplet temperature at the impact was set at 3000 K. A very slight influence of the thermal contact resistance is observed on the spread factor of the droplet in Fig. 13a. The spread factot reaches a maximum of 2.35, which corresponds to a maximum diameter of 119.4 µm after the final spreading, for the different thermal contact resistances.

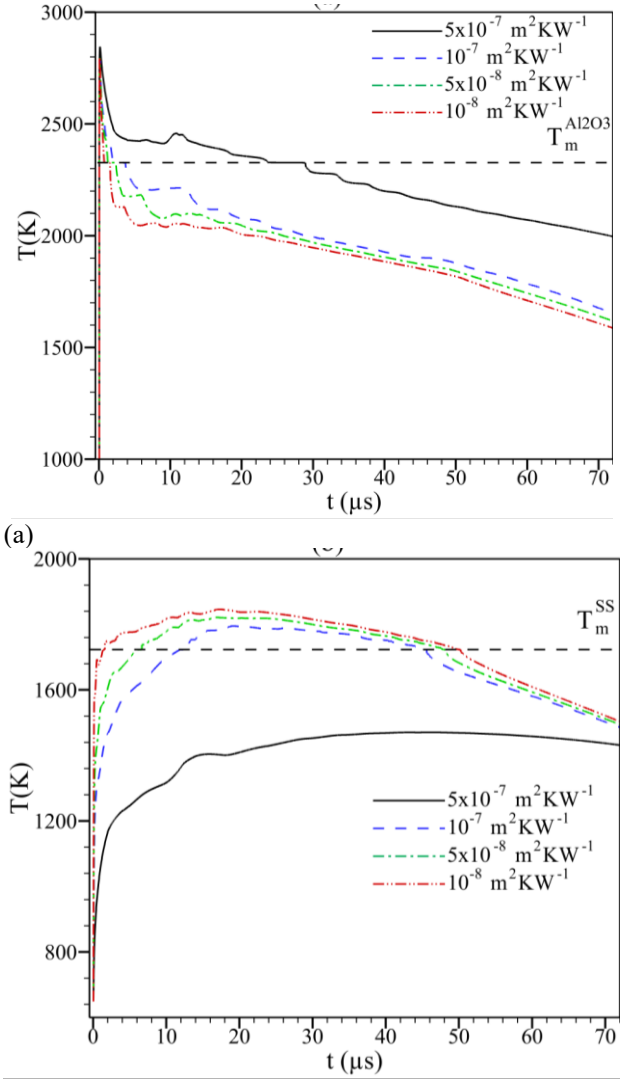

Fig. 14 Temperature history of the lower surface of the droplet (a) and the upper surface of the substrate (b), for different thermal contact resistances

Figure 13b also shows that there is a slight proportionality between height and thermal contact resistance, because the maximum height is 37.95 µm vs 37.18 respectively for $5x10^{-7}\ m^2KW^{-1}$ and $10^{-8}\ m^2KW^{-1}$, this height is reached practically at the same time 4.2 µs vs 4.05 µs. The maximum droplet thickness is significantly influenced by the central counter jet fall on the lower part. As thermal resistance increases, the thickness decreases, with values of 7.3 µm and 9.7 µm corresponding to thermal resistances of $5x10^{-7}\ m^2KW^{-1}$ and $10^{-8}\ m^2KW^{-1}$, respectively. This variation is attributed to the droplet's solidification process, which is highly dependent on thermal contact resistance, as illustrated in image c of Figure 13b at time t=20 µs. In the left part which corresponds to $5x10^{-7}\ m^2KW^{-1}$ the solidification is very slow, which allows the liquid part to move towards the end favoring the flattening of the droplet. Unlike the straight part which corresponds to $10^{-8}\ m^2KW^{-1}$, solidification is faster, which prevents the liquid part from moving towards the end by not promoting flattening of the droplet.

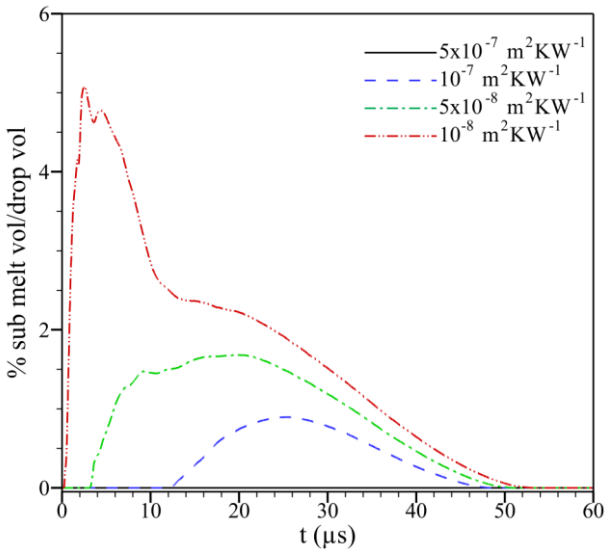

Fig. 15 Temporal evolution of the melted substrate volume, for different thermal contact resistances

Figure 14a shows the temperature history in the bottom surface, at a point that is 10 µm from the center of the droplet, for the different thermal resistances. As can be seen, the solidification occurs just after the impact for the low thermal contact resistances. For a thermal resistance of $5x10^{-7}\ m^2KW^{-1}$, solidification only begins 23.7 µs after impact. Similarly, the cooling rate decreases with higher thermal resistance. Figure 14b illustrates the temperature history of the upper surface of the substrate at a point 10 µm from the center. Higher thermal contact resistance results in reduced heat transfer from the droplet to the substrate, leading to different times required for the temperature to reach the melting point of the substrate: 1.56 µs, 6.56 µs, and 12.42 µs for thermal resistances of $10^{-8}\ m^2KW^{-1}$, $5x10^{-8}\ m^2KW^{-1}$, and $10^{-7}\ m^2KW^{-1}$, respectively. For a resistance of $5x10^{-7}\ m^2KW^{-1}$, the temperature reaches a maximum of 1470 K which is far from the melting point of the substrate.

The influence of thermal contact resistance on the volume of the melted substrate is illustrated in Fig. 15. For high thermal contact resistances, both the maximum melted substrate volume and the melting duration are quite low, specifically 0.89% and 1.68%, with corresponding melting times of 36.4 µs and 47.6 µs for thermal contact resistances of $10^{-7}\ m^2KW^{-1}$ and $5x10^{-8}\ m^2KW^{-1}$ respectively. In these two cases, melting occurs late, following the droplet impact and even slightly after the central counter jet has fallen. No melting of the substrate for $5x10^{-7}\ m^2KW^{-1}$, which can adversely influence the adhesion of the droplet with the substrate.

4. CONCLUSION

This numerical study was performed to analyse the impact of a hollow ceramic droplet (alumina) on a metallic substrate (stainless steel), under plasma projection conditions. The study was realized using a model based on the resolution of the transient equations of fluid dynamics and heat including the solid/liquid phase change, by the

finite volume method in a 2D axisymmetric domain. The droplet/air interface is tracked by the VOF method. A thermal contact resistance was used to model the droplet/substrate interface. The model was fully validated by comparing its results with published experimental ones. The effects of the initial droplet temperature and the thermal contact resistance were analysed. It was discovered that the behaviour of a hollow droplet differs significantly from that of a dense droplet, particularly with the formation of a central counter jet, which influences spreading, solidification, and ultimately the final shape of the splat. With increasing initial droplet temperature, the spreading is more significant, and detachment of a small part is observed. For substrate melting, it is more substantial in volume and time. No melting was observed at low temperatures. Although increasing the thermal contact resistance did not have a significant influence on the droplet spreading, it did cause the droplet to flatten. Conversely, the melting of the substrate became less pronounced, with no melting occurring when thermal contact resistance was high. Finally, through this study it was deduced that the impact of a hollow droplet at a high initial temperature, on a substrate offering low thermal contact resistance, could considerably improve the quality of the coating.

ACKNOWLEDGEMENTS

Thanks for the members of the Laboratory.

CONFLICT OF INTEREST

The authors declare no conflict of interest.

AUTHORS CONTRIBUTION

Mouloud Driouche: Conceptualization, Methodology, Software, Validation, Formal Analysis, Data Curation, Writing – Original Draft Preparation. **Tahar Rezoug:** Methodology, Validation, Formal Analysis, Data Curation, Writing – Review & Editing, Supervision. **Mohamed El Ganaoui:** Formal Analysis, Data Curation, Writing – Review & Editing, Supervision.

REFERENCES

Alavi, S., Passandideh-Fard, M., & Mostaghimi, J. (2012). Simulation of semi-molten particle impacts including heat transfer and phase change. *Journal of Thermal Spray Technology, 21*, 1278–1293. https://doi.org/10.1007/s11666-012-9804-8

An, T., Chen, H., Sang, X., Wang, Y., & Fang, H. (2024). Solidification process of hollow metal droplets impacting a substrate. *International Communications in Heat and Mass Transfer, 159 C*, 108252. https://doi.org/10.1016/j.icheatmasstransfer.2024.108252

ANSYS FLUENT. 16.0, Theory guide, ANSYS, Inc. (2016).

Blanken, N., Saleem, M. S., Thoraval, M. J., & Antonini, C. (2021). Impact of compound drops: a perspective. *Current Opinion in Colloid & Interface Science, 51*, 101389. https://doi.org/10.1016/j.cocis.2020.09.002

Bobzin, K., Heinemann, H., Jasutyn, K., Jeske, S.R., Bender, J., Warkentin, S., Mokrov, O., Sharma, R., & Reisgen, U. (2023). Modeling the droplet impact on the substrate with surface preparation in thermal spraying with SPH. *Journal of Thermal Spray Technology, 32*, 599–608. https://doi.org/10.1007/s11666-023-01534-0

Brackbill, J. U., Kothe, D. B., & Zemach, C. (1992). A continuum method for modeling surface tension. *Journal of Computational Physics, 100*(2), 335-354. https://doi.org/10.1016/0021-9991(92)90240-Y

Chen, D., Feng, A., Wu, F., Wang, T., & Lin, Z. (2024). Experimental study of the collision behavior between moving and sessile droplets on curved surfaces. *Chemical Engineering Science, 299*, 120530. https://doi.org/10.1016/j.ces.2024.120530

Chen, D., Zhang, C., Feng, A., Wang, T., & Lin, Z. (2025). Experimental study on the dynamics of droplet collisions at different viscosities. *Chemical Engineering Science, 307*, 121367. https://doi.org/10.1016/j.ces.2025.121367

Driouche, M., Rezoug, T, & El-Ganaoui, M. (2020). Effect of droplet initial temperature on substrate melting and its re-solidification in plasma spray process. In Chaari, F., Barkallah, M., Bouguecha, A., Zouari, B., Khabou, M. T., Kchaou, M., & Haddar, M. (Eds.), *Advances in Materials, Mechanics and Manufacturing*., Cham; 2020, 123–132. https://doi.org/10.1007/978-3-030-24247-3_14

Driouche, M., Rezoug, T., & El Ganaoui, M. (2019). Numerical study of the melting and resolidification of the substrate during the impact of a ceramic droplet in a plasma spraying process. *The European Physical Journal Applied Physics, 88*, 20901. https://doi.org/10.1051/epjap/2019190279

Emdadi, M., & Pournaderi, P. (2019). Study of droplet impact on a wall using a sharp interface method and different contact line models. *Journal of Applied Fluid Mechanics, 12* (4), 1001-1012. https://doi.org/10.29252/jafm.12.04.29029

Emdadi, M., & Pournaderi, P. (2020). Numerical simulation of conducting droplet impact on a surface under an electric field. *Acta Mechanica, 231*, 1083–1103. https://doi.org/10.1007/s00707-019-02574-w

Goutier, S., Vardelle, M., & Fauchais, P. (2012). Understanding of spray coating adhesion through the formation of a single lamella. *Journal of Thermal Spray Technology, 21*, 522–530. https://doi.org/10.1007/s11666-012-9763-0

Gulyaev, I. P., & Solonenko, O. P. (2013). Hollow droplets impacting onto a solid surface. *Experiments in Fluids, 54*, 1432. https://doi.org/10.1007/s00348-012-1432-z

Gulyaev, I. P., Solonenko, O. P., Gulyaev, P. Y., & Smirnov, A. V. (2009). Hydrodynamic features of the impact of a hollow spherical drop on a flat surface. *Technical Physics Letters, 35*, 885–888. https://doi.org/10.1134/S1063785009100034

Kamnis, S., Gu, S., & Vardavoulias, M. (2011). Numerical study to examine the effect of porosity on in-flight particle dynamics. *Journal of Thermal Spray Technology, 20*, 630–637. https://doi.org/10.1007/s11666-010-9606-9

Keshri, A. K., & Agarwal, A. (2011). Splat morphology of plasma sprayed aluminum oxide reinforced with carbon nanotubes: A comparison between experiments and simulation. *Surface and Coatings Technology, 206*, 338-347. https://doi.org/10.1016/j.surfcoat.2011.07.025

Kumar, A., Gu, S., & Kamnis, S. (2012). Simulation of impact of a hollow droplet on a flat surface. *Applied Physics A, 109*, 101-109. https://doi.org/10.1007/s00339-012-7043-y

Kumar, A., Gu, S., Tabbara, H., & Kamnis, S. (2013). Study of impingement of hollow ZrO2 droplets onto a substrate. *Surface and Coatings Technology, 220*, 164-169. https://doi.org/10.1016/j.surfcoat.2012.08.061

Labergue, A., Gradeck, M., & Lemoine, F. (2015). Comparative study of the cooling of a hot temperature surface using sprays and liquid jets. *International Journal of Heat and Mass Transfer, 81*, 889-900. https://doi.org/10.1016/j.ijheatmasstransfer.2014.11.018

Latka, L., Pawłowski, L., Winnicki, M., Sokołowski, P., Małachowska, M., & Kozerski, S. (2020). Review of functionally graded thermal sprayed coatings. *Applied Sciences, 10*(15), 5153. https://doi.org/10.3390/app10155153

Li, C. J., Li, C. X., Yang, G. J., & Wang, Y. Y. (2006). Examination of substrate surface melting-induced splashing during splat formation in plasma spraying. *Journal of Thermal Spray Technology, 15*, 717-724. https://doi.org/10.1361/105996306X146947

Li, L., Wang, X. Y., Wei, G., Vaiday, A., Zhang, H., & Sampath, S. (2004). Substrate melting during thermal spray splat quenching. *Thin Solid Films, 468*, 113-119. https://doi.org/10.1016/j.tsf.2004.05.073

Niu, J., Sang, W., Li, D., Guo, Q., Qiu, A., & Shi, M. (2023). Fast prediction of multiple parameters related to iced airfoil based on POD and kriging methods. *Journal of Applied Fluid Mechanics, 16*(2), 325-336. https://doi.org/10.47176/jafm.16.02.1379

Pasandideh-Fard, M., Qiao, Y. M., Chandra, S., & Mostaghimi, J. (1996). Capillary effects during droplet impact on a solid surface. *Physics of Fluids, 8,* 650–659. https://doi.org/10.1063/1.868850

Patel, V., Yadav, A., & Winczek, J. (2022). Computational study of the effect of spray parameters on adhesion of splat on the stainless street substrate during the impact of molten zirconia droplet. *Heat and Mass Transfer, 58*, 1365-1380. https://doi.org/10.1007/s00231-022-03184-4

Safaei, H., & Emami M. D. (2017). Numerical and analytical simulation of the production process of ZrO2 hollow particles. *The European Physical Journal Plus, 132*, 508. https://doi.org/10.1140/epjp/i2017-11768-1

Safaei, H., Emami, M. D., Jazi, H. S., & Mostaghimi, J. (2017). application of compressible volume of fluid model in simulating the impact and solidification of hollow spherical ZrO2 droplet on a surface. *Journal of Thermal Spray Technology, 26*, 1959-1981. https://doi.org/10.1007/s11666-017-0632-8

Shen, M., Li, B. Q., & Bai, Y. (2020). Numerical modeling of YSZ droplet impact/spreading with solidification microstructure formation in plasma spraying. *International Journal of Heat and Mass Transfer, 150*, 119267. https://doi.org/10.1016/j.ijheatmasstransfer.2019.119267

Shigeru, K., & Atsushi, H. (1974). A study of the bonding mechanism of sprayed coatings. *Journal of Vacuum Science & Technology, 11*(4), 747-753. https://doi.org/10.1116/1.1312746

Solonenko, O. P., Gulyaev, I. P., & Smirnov, A. V. (2008a). Plasma processing and deposition of powdered metal oxides consisting of hollow spherical particles. *Technical Physics Letters, 34*, 1050-1052. https://doi.org/10.1134/S1063785008120183

Solonenko, O. P., Smirnov, A. V., & Gulyaev, I. P. (2008b). *Spreading and solidification of hollow molten droplet under its impact onto substrate: Computer simulation and experiment*. AIP Conference Proceedings, 982, 561-568. https://doi.org/10.1063/1.2897859

Tejero-Martin, D., Rezvani Rad, M., McDonald, A., & Hussain, T. (2019). Beyond traditional coatings: a review on thermal-sprayed functional and smart coatings. *Journal of Thermal Spray Technology, 28*, 598–644. https://doi.org/10.1007/s11666-019-00857-1

Voller, V. R., & Prakash, C. (1987). A fixed grid numerical modelling methodology for convection-diffusion mushy region phase-change problems. *International Journal of Heat and Mass Transfer, 30*(8), 1709-1719. https://doi.org/10.1016/0017-9310(87)90317-6

Xiaogang, L., Yanhua, W., Zhongyi W, Xinquan, Z., Jing, Z., & Haiou, S. (2023). Modeling the impingement deformation and solidification of a hollow zirconia droplet onto a dry substrate and solidified layer. *AIP Advances, 13*(3), 035213. https://doi.org/10.1063/5.0133936

Xu, M., Zhang, J., & Chen, R. Y. (2022). Cooling effect of droplet impacting on heated solid surface. *International Journal of Heat and Mass Transfer, 183*(A), 122070. https://doi.org/10.1016/j.ijheatmasstransfer.2021.122070

Zhong, Y., Dong, X., Yin, Z., & Fang, H. (2020). Theoretical design of inkjet process to improve delivery efficiency. *Journal of Applied Fluid Mechanics, 13*(1), 275-286. https://doi.org/10.29252/jafm.13.01.30395